

Generalized Kirchoff's Current and Voltage Law Formulation for Coupled Circuit–Electromagnetic Simulation With Surface Integral Equations

Yong Wang, Dipanjan Gope, *Student Member, IEEE*, Vikram Jandhyala, *Senior Member, IEEE*, and C.-J. Richard Shi, *Senior Member, IEEE*

Abstract—In this paper, a new formulation for coupled circuit–electromagnetic (EM) simulation is presented. The formulation employs full-wave integral equations to model the EM behavior of two- or three-dimensional structures while using modified nodal analysis to model circuit interactions. A coupling scheme based on charge and current continuity and potential matching, realized as a generalization of Kirchoff's voltage and current laws, ensures that the EM and circuit interactions can be formulated as a seamless system. While rigorous port models for EM structures can be obtained using the approach discussed herein, it is shown that the coupling paradigm can reveal additional details of the EM–circuit interactions and can provide a path to analysis-based design iteration.

Index Terms—Coupled circuit–electromagnetic (EM) simulation, method of moments (MoM), signal integrity, surface integral equation.

I. INTRODUCTION

WITH THE rapidly increasing interest in applications such as RF wireless communication and high-speed data processing, electronic systems are required to work at progressively higher frequencies [1]. As the operating frequencies enter gigahertz range, phenomena such as crosstalk, power and ground-plane voltage bounce, substrate losses, etc. can no longer be neglected. In order to design high-performance systems with fast time to market, it is essential to be able to analyze whole or part of the system at one fundamentally deeper level of physics: distributed electromagnetic (EM) field analysis needs to be rigorously and seamlessly included as an addition to traditional circuit simulation.

In the existing literature, several methods have been developed to model and simulate coupled circuit–EM problems. Those based on finite difference time domain (FDTD) [2]–[4] are effective for time-domain analysis. For broad-band simulation, the FDTD can be used to obtain frequency-domain results via a Fourier transform. However, it is not a direct

frequency-domain method, and it also requires dispersive/frequency-dependent parameters to be represented in the time domain in order to model losses and frequency-dependent behavior, accomplished through recursive convolutions and similar methods. Furthermore, FDTD requires the discretization of the three-dimensional (3-D) space where the object under study resides, which can lead to substantially more system unknowns than in surface-based methods [5]. The finite-element method (FEM) has been applied to both time- and frequency-domain coupled circuit–EM simulation using schemes including port models [6] via paralleling each coupling circuit element to an FEM edge [7] or through a fully coupled approach [8], as has been the transmission-line method [9]. Analytical approaches [10] and simpler transmission lines are usually much faster than the numerical-based methods and can be easily coupled to circuit simulation. However, they are not general enough for analyzing irregular structures.

In recent years, methods based on integral equations have gained importance. Among them, the partial-element equivalent-circuit (PEEC) approach [11] has been widely used to study coupled circuit–EM problems. Very recently, nonorthogonal and generalized PEEC methods have been developed [12], [13]. By representing all the interactions using equivalent SPICE-compatible resistor–inductor–capacitor (RLC) elements and controlled sources, PEEC can solve the coupled circuit–EM problem using a traditional SPICE-like circuit simulator. However, due to the dense nature of the interactions and the fact that SPICE is tuned for solving sparse matrices, direct PEEC is limited to problems with a relatively small number of unknowns [14], although recently, fast methods in conjunction with PEEC are being developed [15], [16]. The PEEC method itself was inspired by EM integral equations. These equations, solved by the method of moments (MoM) [17] with appropriate basis functions, can be used for distributed effects simulation of arbitrarily shaped structures.

When nontrivial lumped circuits are simultaneously present, previous work can only solve the coupled problem based on port models through several steps: port parameters are calculated using an EM simulator first, curve-fitting or model order-reduction techniques are then used to generate an equivalent-circuit model, followed by circuit simulation to estimate complete electrical performance of the system. The port-model-based approach has several limitations: first, for complex multiport structures with frequency-dependent material properties, deriving the equivalent passive network within a

Manuscript received July 28, 2003; revised February 3, 2004. This work was supported in part by the Defense Advanced Research Projects Agency–Micro Technology Office under NeoCAD Grant N66001-01-1-8920, by the National Science Foundation (NSF) under CAREER Grant ECS-0093102, by the NSF–Semiconductor Research Cooperation under Mixed-Signal Initiative Grant CCR-0120371, and by the Ansoft Corporation under a grant.

The authors are with the Electrical Engineering Department, University of Washington, Seattle, WA 98195-2500 USA (e-mail: yongw@ee.washington.edu; dips@u.washington.edu; jandhyala@ee.washington.edu; shi@ee.washington.edu).

Digital Object Identifier 10.1109/TMTT.2004.830482

given accuracy is still an area of current research [18]. Second, after the EM structure is converted to a port model, information about the details of the EM-field distribution in the structure will be lost, such information could otherwise provide useful insights into the problem under study and be useful in design iterations. Third, the port-model approach, when used with a fast iterative solver, needs to solve the EM system repeatedly, i.e., for each port, which could be very expensive when both the number of ports and number of unknowns are large.

This paper presents a new and complementary approach to the formulation and solution of the coupled circuit–EM problem. EM conducting structures and lumped-element circuits are formulated jointly using one system matrix in a form amenable to existing fast iterative numerical solvers such as those based on the fast multipole method [19], fast Fourier transform (FFT) method [20], and low-rank decomposition [21], as well as emerging fast direct solvers [22]. Solving the EM and circuit simultaneously not only permits more detailed field information, but also obviates the necessity of generating port models and, thus, automates the design flow. The proposed method, originally presented by the authors as an idea at a recent conference [23], is detailed and advanced herein, and applied to several microelectronic problems. The technique is inherently hierarchical and provides seamless transitions between circuit and EM depending on the level of details required.

The EM formulation used in this paper is a full-wave MoM approach using surface triangular tessellations. Since Rao–Wilton–Glisson (RWG) basis functions [24] associated with triangular meshes do not make assumptions about current flow directions as the classical volumetric PEEC does, the adopted approach is suitable to model arbitrarily shaped structures often found in microwave and RF applications. The presented formulation employs a surface impedance approximation that is valid at high frequencies for thin and thick conductors. Although not presented here, for a complete broad-band solution, frequency-dependent effects can be modeled via employing lossy media’s Green’s functions in a two-region formulation without frequency-dependent meshing [25].

For the circuit subsystem, the standard modified nodal analysis (MNA) matrix is formulated. Kirchoff’s current law (KCL) is enforced for each circuit node and Kirchoff’s voltage law (KVL) is applied to branches containing voltage sources. Areas of EM structures where the circuit connections are made are defined as *contact* regions. Associated with each *contact* are coupling currents that are introduced as additional system unknowns. The coupling scheme is based on charge and current continuity equations and potential matching with the assumption that circuit voltage is equal to the EM scalar potential at a *contact* region.

The remainder of this paper is organized as following. Section II introduces the formulation of surface-based electric field integral equations (EFIEs) for EM structures, and MNA equations for lumped-element circuits. Implementation of the coupled method using RWG basis functions is presented in Section III. Section IV discusses port-model derivation and comparison between the port-model and coupled approaches. Numerical

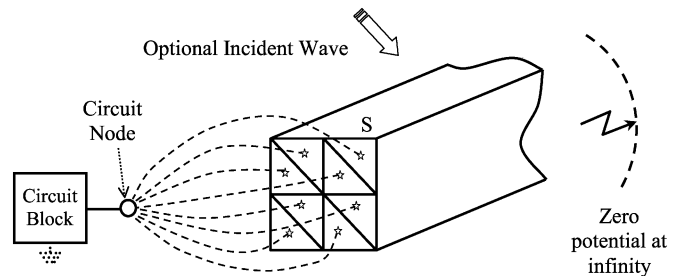


Fig. 1. Arbitrary lumped circuit connected through a contact to a 3-D geometric object.

examples for a low-noise amplifier (LNA), power/ground-plane bounce modeling are given in Section V. Section VI discusses conclusions.

II. COUPLED CIRCUIT–EM FORMULATION

This section presents a generalized KCL–KVL formulation for simulation of coupled circuit–EM problems. A typical high-speed microelectronic system layout consists of both lumped circuits and sections requiring distributed EM simulation. For modeling purposes, the circuit section is abstracted by a topology-based domain, wherein signals propagate along idealized conduction paths between lumped-circuit elements, while the EM section is represented by a geometry-based domain, wherein signals propagate in 3-D space and materials. The two domains couple to each other through contact interfaces where a circuit node is associated with an EM contact surface. As will be shown in this paper, this interface can be rigorously defined using a generalized version of Kirchoff’s voltage and current laws.

Consider Fig. 1, which shows a 3-D geometric object connected through a *contact* to lumped circuits and, optionally, illuminated by incident fields.

The boundary condition for the electric field on the surface S of the object is

$$(\mathbf{E}^s(\mathbf{J}) + \mathbf{E}^i)_{\text{tan}} = Z_s \mathbf{J} \quad (1)$$

where \mathbf{E}^s is the scattered electric field produced by the induced equivalent-surface current \mathbf{J} , \mathbf{E}^i is the incident electric field, subscript tan denotes the tangential components on S , Z_s represents the surface impedance, and its value is

$$Z_s = \sqrt{j\omega\mu/\sigma} \quad (2)$$

where ω is angular frequency, and μ and σ are the permittivity and conductivity of the material, respectively. Note that surface impedance is a valid approximation to the behavior of fields internal to conductors only for frequencies where the skin depth is smaller than the dimension of the cross section of conductors. At lower frequencies, if a surface integral formulation is used, more accurate modeling of the lossy media Green’s function within the conductor is required, as discussed in [26]. In terms of potentials, the electric field can be written as

$$\mathbf{E}^s(\mathbf{J}) = -j\omega\mathbf{A} - \nabla\Phi \quad (3)$$

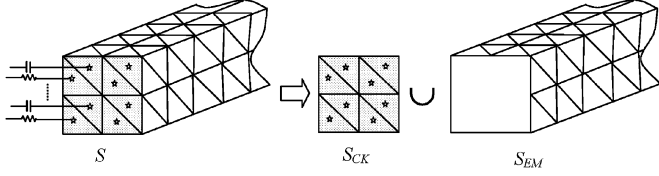


Fig. 2. Concept of surface contact.

where the vector potential \mathbf{A} is defined as

$$\mathbf{A}(\mathbf{r}) = \frac{\mu}{4\pi} \int_S \frac{e^{-jk|\mathbf{r}-\mathbf{r}'|} \mathbf{J}(\mathbf{r}')}{|\mathbf{r}-\mathbf{r}'|} ds' \quad (4)$$

the scalar potential Φ is defined as

$$\Phi(\mathbf{r}) = \frac{1}{4\pi\epsilon} \int_S \frac{e^{-jk|\mathbf{r}-\mathbf{r}'|} \rho(\mathbf{r}')}{|\mathbf{r}-\mathbf{r}'|} ds' \quad (5)$$

where \mathbf{r} and \mathbf{r}' are observation and source locations, respectively, \mathbf{J} and ρ represent the equivalent surface current density and surface charge density, respectively, and μ, ϵ, k are the permeability, permittivity, and wavenumber, respectively, of the homogeneous medium enclosing the object.

The concept of a *contact* is introduced in Fig. 2, where surface S is divided into two subsurfaces, denoted by S_{CK} and S_{EM} such that

$$S_{EM} \cup S_{CK} = S \quad (6a)$$

and

$$S_{EM} \cap S_{CK} = \phi. \quad (6b)$$

On S_{EM} , the standard continuity equation relating the surface current density \mathbf{J} and surface charge density ρ holds as follows:

$$\nabla_s \cdot \mathbf{J}(\mathbf{r}) + j\omega\rho(\mathbf{r}) = 0 \quad \forall \mathbf{r} \in S_{EM} \quad (7a)$$

or

$$\rho(\mathbf{r}) = -\nabla_s \cdot \mathbf{J}(\mathbf{r}) / (j\omega) \quad \forall \mathbf{r} \in S_{EM} \quad (7b)$$

where ∇_s represents the surface divergence.

On S_{CK} , the continuity equation is altered due to the existence of injected circuit currents. This current introduces an additional source term in the continuity equation and, thus, affects the distribution of both surface currents and surface charges. Let S_{CK} be comprised of M disjoint surfaces $S_{CK}^m, m = 1, \dots, M$, each such unique subsurface S_{CK}^m is termed one of M *contacts*. On S_{CK}^m , the modified continuity equation has the following form:

$$\nabla_s \cdot \mathbf{J}(\mathbf{r}) + j\omega\rho(\mathbf{r}) = J_c^m(\mathbf{r}) \quad \forall \mathbf{r} \in S_{CK}^m \quad (8a)$$

or

$$\rho(\mathbf{r}) = \left(J_c^m(\mathbf{r}) - \nabla_s \cdot \mathbf{J}(\mathbf{r}) \right) / (j\omega), \quad \forall \mathbf{r} \in S_{CK}^m; \quad m = 1, \dots, M \quad (8b)$$

where J_c^m represents the scalar volumetric current density produced on S_{CK}^m via a circuit interconnection, and ρ represents total surface charge density on S_{CK} .

Substitute (6a)–(8b) into (3)–(5), we have

$$\begin{aligned} \mathbf{E}^s(\mathbf{J}) = & -\frac{j\omega\mu}{4\pi} \int_S \frac{e^{-jk|\mathbf{r}-\mathbf{r}'|} \mathbf{J}(\mathbf{r}')}{|\mathbf{r}-\mathbf{r}'|} ds' \\ & -\nabla \frac{1}{4\pi\epsilon j\omega} \int_S \frac{e^{-jk|\mathbf{r}-\mathbf{r}'|} \nabla' \cdot \mathbf{J}(\mathbf{r}')}{|\mathbf{r}-\mathbf{r}'|} ds' \\ & -\nabla \frac{1}{4\pi\epsilon} \sum_{m=1}^M \int_{S_{CK}^m} \frac{e^{-jk|\mathbf{r}-\mathbf{r}'|} J_c^m(\mathbf{r}')}{j\omega|\mathbf{r}-\mathbf{r}'|} ds'. \end{aligned} \quad (9)$$

The last two terms represent the contribution to the field produced by the gradient of the scalar potential, which, in turn, is produced by the equivalent surface charge density. The charge density itself is produced by $-\nabla_s \cdot \mathbf{J} / (j\omega)$ over S_{EM} , and by $(J_c^m - \nabla_s \cdot \mathbf{J}) / (j\omega)$ over S_{CK}^m . Therefore, the current density introduced by the circuit interconnection produces an additional source or sink of charge that alters the scalar potential and the resulting electric field.

The current density J_c^m is a system unknown that is determined by the solution of the coupled circuit-EM system. An additional system equation can also be constructed, which is based on a generalized KVL that equates the scalar potential produced on electrically small contacts S_{CK}^m to the voltage of the circuit node associated with the interconnection at S_{CK}^m as follows:

$$\begin{aligned} V_n = & \frac{-1}{4\pi\epsilon j\omega} \left(\int_S \frac{e^{-jk|\mathbf{r}-\mathbf{r}'|} \nabla' \cdot \mathbf{J}(\mathbf{r}')}{|\mathbf{r}-\mathbf{r}'|} ds' \right. \\ & \left. - \sum_{m=1}^M \int_{S_{CK}^m} \frac{e^{-jk|\mathbf{r}-\mathbf{r}'|} J_c^m(\mathbf{r}')}{j\omega|\mathbf{r}-\mathbf{r}'|} ds' \right), \\ & \forall \mathbf{r} \in S_{CK}^n; \quad n = 1, \dots, M \end{aligned} \quad (10)$$

where V_n corresponds to the node voltage associated with a circuit node connected to *contact*.

The *contact*, as defined above, is inherently an electrically small surface, i.e., its dimensions are small compared to the wavelength of signals in a microelectronic system. Larger *contacts* can be defined by associating several circuit nodes with neighboring contact regions, thereby not enforcing erroneous constant potential over electrically large regions.

As can be seen from (10), the calculation of the scalar potential at the *contacts* assumes the potential at infinity is zero. Although the ground node can be chosen randomly in a pure circuit problem, in a coupled circuit-EM formulation, specifying a circuit node to be a ground node indicates this node has the same potential as the EM scalar potential at infinite distance. In the coupled formulation, there is no requirement to define a circuit ground and, in fact, every node has an associated KCL (which is not possible in a pure circuit problem since one of them will be redundant). Thus, there is one unambiguous ground (infinity) definition in the entire problem.

The final self-consistency condition, in addition to scalar potential matching, is a generalized KCL, which ensures that the coupling current will contribute one additional term I_c^n to the

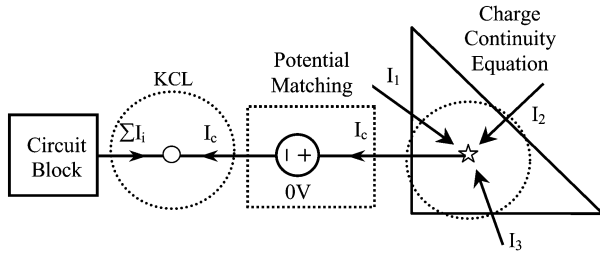


Fig. 3. Connection scheme for EM and circuit interface.

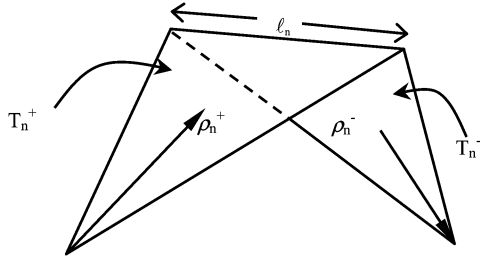


Fig. 4. Definition of RWG basis function.

KCL-based circuit equation associated with circuit node n as follows:

$$\sum_{i=1}^B I_i + I_C^m = 0 \quad (11)$$

where I_i is the current of the i th branch, and B is the total number of circuit branches connected to circuit node n . Fig. 3 shows the connection scheme for the EM–circuit interface.

We notice that whereas other approaches such as delta gap methods or wire basis functions [27] can be used to describe the coupling between the circuit and EM, they often need artificial parameters such as basis-function lengths, directions, and radii that are not consistent with topology-only circuit sections.

III. INTEGRAL EQUATION WITH RWG BASIS FUNCTIONS

The self-consistent coupled circuit–EM equations described in Section II are valid for arbitrary basis functions for modeling surface currents using surface integral formulations. Here, the method is expressed in more detail for the popular edge-based RWG spatial basis functions [24] that rely on a triangular tessellation of the surface S . An RWG function $\mathbf{f}_n(\mathbf{r})$, defined over two triangles with a common edge n , used to approximate the spatial distribution of current density has the well-known form

$$\mathbf{f}_n(\mathbf{r}) = \begin{cases} \frac{l_n}{2A_{n+}} \boldsymbol{\rho}_{n+}, & \mathbf{r} \in T_{n+} \\ \frac{l_n}{2A_{n-}} \boldsymbol{\rho}_{n-}, & \mathbf{r} \in T_{n-} \end{cases} \quad (12)$$

where l_n is the length of the n th edge, $A_{n\pm}$ is the area of triangle $T_{n\pm}$, and $\boldsymbol{\rho}_{n\pm}$ is the vector pointing to or from location \mathbf{r} in triangle $T_{n\pm}$ with respect to the node opposite the edge. Fig. 4 illustrates the definition of RWG basis functions.

As a consequence of the above form, the charge density in each pair of triangles is modeled as a piecewise constant as follows:

$$\nabla \cdot \mathbf{f}_n(\mathbf{r}) = \begin{cases} \frac{l_n}{A_{n+}}, & \mathbf{r} \in T_{n+} \\ -\frac{l_n}{A_{n-}}, & \mathbf{r} \in T_{n-}. \end{cases} \quad (13)$$

The surface current density is expanded using RWG functions as

$$\mathbf{J}(\mathbf{r}) \cong \sum_{i=1}^{N_e} I_i \mathbf{f}_i(\mathbf{r}) \quad (14)$$

where I_i represents the coefficient of the i th RWG basis function, and N_e is the total number of nonboundary edges. For consistency with RWG basis functions, the charge associated with the coupling current is modeled using piecewise constant functions h (that have a value of unity on a given triangle and zero elsewhere) over each contact triangle

$$J_{c,n}^m(\mathbf{r}) \cong \sum_{m=1}^M \sum_{n=1}^{N_{p,CK}^m} J_n^m h_n^m(\mathbf{r}). \quad (15)$$

Equation (9) is then expressed as

$$\begin{aligned} \mathbf{E}^s(\mathbf{r}) = & -j\omega \frac{\mu}{4\pi} \sum_{i=1}^{N_e} I_i \int_{T_{i+} \cup T_{i-}} \frac{e^{-jk|\mathbf{r}-\mathbf{r}'|} \mathbf{f}_i(\mathbf{r}')}{|\mathbf{r}-\mathbf{r}'|} ds' \\ & + \nabla \frac{1}{4\pi\epsilon} \sum_{i=1}^{N_e} I_i \int_{T_{i+} \cup T_{i-}} \frac{e^{-jk|\mathbf{r}-\mathbf{r}'|} \nabla_s \cdot \mathbf{f}_i(\mathbf{r}')}{j\omega|\mathbf{r}-\mathbf{r}'|} ds' \\ & - \nabla \frac{1}{4\pi\epsilon} \sum_{m=1}^M \sum_{n=1}^{N_{p,CK}^m} J_n^m \int_{T_{n,CK}^m} \frac{e^{-jk|\mathbf{r}-\mathbf{r}'|} h_n^m(\mathbf{r}')}{j\omega|\mathbf{r}-\mathbf{r}'|} ds' \end{aligned} \quad (16)$$

where N_e is the total number of nonboundary edges, $N_{p,CK}^m$ is total number of triangles on *contact* m , and $T_{n,CK}^m$ denotes the n th triangle on *contact* m that is used for circuit connection. Also, T_{i+} and T_{i-} are the positive and negative triangles associated with the i th RWG function. To solve for the unknown coefficients, the expression in (16) is substituted into (1) and tested with the RWG functions to yield

$$\begin{aligned} j\omega \langle \mathbf{f}_n, \mathbf{A}(\mathbf{r}) \rangle_{\text{tan}} + \langle \mathbf{f}_n, \nabla \Phi(\mathbf{r}) \rangle_{\text{tan}} \\ = -\langle \mathbf{f}_n, Z_s \mathbf{J} \rangle_{\text{tan}} + \langle \mathbf{f}_n, \mathbf{E}^i \rangle_{\text{tan}}, \quad n = 1, \dots, N_e \end{aligned} \quad (17)$$

where $\langle \cdot, \cdot \rangle$ denotes a spatial dot product, and testing of the vector potential yields

$$\langle \mathbf{f}_n, \mathbf{A}(\mathbf{r}) \rangle = \frac{\mu}{4\pi} \sum_{i=1}^{N_e} I_i \left\langle \mathbf{f}_n, \int_{T_{i+} \cup T_{i-}} \frac{e^{-jk|\mathbf{r}-\mathbf{r}'|} \mathbf{f}_i(\mathbf{r}')}{|\mathbf{r}-\mathbf{r}'|} ds' \right\rangle. \quad (18)$$

The testing of the scalar potential is the result of the sum of two potential contributions, Φ_s from the EM surface current

$$\langle \mathbf{f}_n, \nabla \Phi_s(r) \rangle = \frac{-1}{4\pi\epsilon} \sum_{i=1}^{N_e} I_i \times \left\langle \nabla \cdot \mathbf{f}_n, \int_{T_{i+} \cup T_{i-}} \frac{e^{-jk|\mathbf{r}-\mathbf{r}'|} \nabla_s \cdot \mathbf{f}_i(\mathbf{r}')}{j\omega|\mathbf{r}-\mathbf{r}'|} \right\rangle \quad (19)$$

and Φ_c from the coupling current

$$\langle \mathbf{f}_n, \nabla \Phi_c(r) \rangle = \frac{1}{4\pi\epsilon} \sum_{m=1}^M \sum_{i=1}^{N_{p,\text{CK}}^m} J_i^m \times \left\langle \nabla \cdot \mathbf{f}_n, \int_{T_{i,\text{CK}}^m} \frac{e^{-jk|\mathbf{r}-\mathbf{r}'|} h_i^m(\mathbf{r}')}{j\omega|\mathbf{r}-\mathbf{r}'|} \right\rangle. \quad (20)$$

The surface impedance contribution is local and has nonzero values only for those combinations of basis and testing functions that share at least one triangle. Therefore, the contribution is a sparse matrix where each column has, at most, five nonzero entries as follows:

$$\langle \mathbf{f}_n, Z_s \mathbf{J} \rangle = Z_s \sum_{i=1}^{N_e} I_i \langle \mathbf{f}_n, \mathbf{f}_i \rangle, \quad n, i \text{ share a common triangle.} \quad (21)$$

Finally, any incident electric field is tested as in the term $\langle \mathbf{f}_n, \mathbf{E}^i \rangle$.

The next set of equations is obtained by enforcing

$$V_n = \frac{-1}{4\pi\epsilon j\omega} \times \left(\sum_{i=1}^{N_e} I_i \left\langle h_n^m, \int_{T_{i+} \cup T_{i-}} \frac{e^{-jk|\mathbf{r}-\mathbf{r}'|} \nabla_s \cdot \mathbf{f}_i(\mathbf{r}')}{|\mathbf{r}-\mathbf{r}'|} ds' \right\rangle + \sum_{m=1}^M \sum_{k=1}^{N_{p,\text{CK}}^m} J_k^m \int_{S_{\text{CK}}^m} \frac{e^{-jk|\mathbf{r}-\mathbf{r}'|} h_n^m(\mathbf{r}')}{|\mathbf{r}-\mathbf{r}'|} ds' \right) \quad \forall \mathbf{r} \in S_{\text{CK}}^m; \quad n = 1, \dots, M \quad (22)$$

and by enforcing (15). Substituting (19)–(22) in (18) leads to the matrix format of the coupled circuit-EM system

$$\begin{bmatrix} \mathbf{Z}_{11} & \mathbf{Z}_{12} & \mathbf{0} \\ \mathbf{Z}_{21} & \mathbf{Z}_{22} & \mathbf{C} \\ \mathbf{0} & \mathbf{C}^T & \text{MNA} \end{bmatrix} \begin{bmatrix} \mathbf{i} \\ \mathbf{j}_c \\ \mathbf{ckt} \end{bmatrix} = \begin{bmatrix} \mathbf{v}_{\text{em}} \\ \mathbf{0} \\ \mathbf{v}_{\text{ckt}} \end{bmatrix} \quad (23)$$

where \mathbf{Z}_{11} is the regular MoM matrix whose elements can be interpreted as equivalent partial impedances if a comparison with a surface-based PEEC is desired. The partial inductances, capacitances, and resistances are equivalent to the terms in (19)–(21). The remaining three dense EM matrices define the *contact*. Matrix \mathbf{Z}_{12} represents the scalar potential contribution due to the coupling current at S_{EM} , and matrix \mathbf{Z}_{21} denotes the potential contribution from the EM surface current

at S_{CK} . Finally, matrix \mathbf{Z}_{22} represents the scalar potential contribution to S_{CK} due to coupling currents. This two-by-two system is a self-consistent definition of the EM interactions with a circuit section. To complete the coupled formulation, a sparse rectangular matrix \mathbf{C} is introduced as connection matrix to enforce generalized KCL and KVL. This matrix has one nonzero element per row to select the potential of the circuit node associated with a *contact* triangle. The transpose matrix \mathbf{C}^T selects the coupling current and adds it to the KCL equation of the circuit node at the *contact*. The **MNA** matrix represents circuit interactions for linear RLC elements and the linearized small-signal models of nonlinear elements such as diodes and transistors. The system unknowns \mathbf{i} , \mathbf{j}_c , and \mathbf{ckt} relate to surface equivalent currents, coupling currents, and circuit voltages/currents, respectively. The right-hand-side excitation vector consists of the tested incident EM field \mathbf{v}_{em} , the strengths of independent voltage, and current sources \mathbf{v}_{ckt} [28].

IV. PORT MODEL VERSUS COUPLED SOLUTION

The port model is a widely used approach for circuit designers to include EM effects. Here, we first show how the coupled solver can be used to generate port models, and then we give a comparison between the port-model and coupled approach to show that coupled solver has advantages in terms of simulation cost and automation.

In addition to being used as a fully coupled solver, the formulation discussed in Section III can also be used in a manner similar to port-model approaches. Equations (15) and (22) permit sufficient flexibility in solution in order to aid iterations in circuit design. When structures to be analyzed with EM analysis remain unchanged and circuit parameters and topologies vary during design iterations, an *EM contact model* is generated. By combining the first two equations and unknowns, (23) can be rewritten as

$$\begin{pmatrix} \mathbf{EM} & \mathbf{C}' \\ \mathbf{C}^T & \text{MNA} \end{pmatrix} \begin{pmatrix} \mathbf{i}' \\ \mathbf{ckt} \end{pmatrix} = \begin{pmatrix} \mathbf{v}_{\text{em}'} \\ \mathbf{v}_{\text{ckt}} \end{pmatrix} \quad (24)$$

where \mathbf{EM} contains \mathbf{Z}_{11} , \mathbf{Z}_{12} , \mathbf{Z}_{21} , and \mathbf{Z}_{22} in (23), \mathbf{C}' , \mathbf{i}' , and $\mathbf{v}_{\text{em}'}$ are extensions of their corresponding entry in (23). In (24), the EM surface current and coupling current unknowns \mathbf{i}' can be eliminated from the first set of equations and the rest of the system can be written in the Schur complement form

$$(\text{MNA} - \mathbf{C}'^T \mathbf{EM}^{-1} \mathbf{C}') \mathbf{ckt} = \mathbf{v}_{\text{ckt}} - \mathbf{C}'^T \mathbf{EM}^{-1} \mathbf{v}_{\text{em}'}. \quad (25)$$

Therefore, the formal inversion of the matrix \mathbf{EM} only needs to be done once as long as the EM structures do not change. For large-sized EM problems, the equivalent of the inversion is obtained by iteratively solving the EM system with each of the contacts excited independently. The *EM contact model* can, therefore, be obtained through exciting each contact and using an iterative solver, or through the formal inversion shown in (25).

The *EM contact model* ultimately permits the EM structure to be represented in an MNA-compatible element-stamping

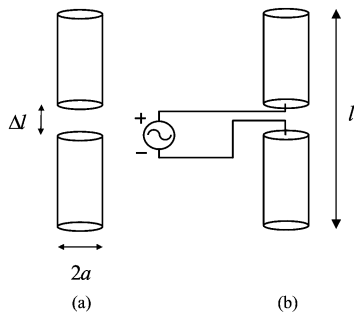


Fig. 5. Illustration of a short-wire antenna of length l and radius a ($l/2a = 74.2$). (a) Classic MoM solution. (b) Coupled circuit-EM solution.

format $\mathbf{C}'^T \mathbf{EM}^{-1} \mathbf{C}'$ and the incident EM wave in the equivalent-circuit excitation format $\mathbf{C}'^T \mathbf{EM}^{-1} \mathbf{v}_{em}$. The advantage of the above nodal contact model compared to the traditional port model is that it eliminates the intermediate step of constructing an equivalent circuit with its associated cost, accuracy limitations, and complexity in terms of ensuring passivity.

The advantages of coupled formulation over port-model methods lie in several areas. First, computation cost for port-model extraction, assuming a standard or fast iterative solver, increases linearly with the number of ports. Consider an N -port EM structure as an example, column i of its Y -parameter matrix needs to be calculated with port i connected to 1 V, while the rest of ports are grounded. Thus, an N -port structure will necessitate solving the system for N times. Since the coupled solver only needs to solve the system equations (23) once, the port-model approach will be computationally more expensive than the coupled method. Second, the coupled solver can reveal the distributed field information more easily. Distributed field information is important for layout-based circuit design. In the coupled formulation, since surface currents are formulated as system unknowns, field distribution will be just a simple post-processing after the system is solved. In the port-model approach, to derive distributed field information, one has to either solve the problem again with the derived port voltage and current or use complex bookkeeping and superposition to recalculate the field distribution. Coupled formulation also automates the process to consider EM effects during circuit design.

V. NUMERICAL RESULTS

A fully coupled circuit-EM simulator has been developed based on the above-described approach. The first example is a validation test against the classical MoM. As shown in Fig. 5, the input admittance of a center-fed antenna is simulated [17].

In Fig. 5, the short-wire antenna under consideration is of length l and radius a such that the ratio of the length and diameter is 74.2 and $\Delta l \ll l$. The input admittance is first simulated using our in-house MoM solver, employing a delta-gap excitation at its center, as shown in Fig. 5(a). The antenna is then excited at its center by a circuit voltage source and our coupled solver is used to solve for the input impedance, as shown in Fig. 5(b). The simulation results from both methods are illustrated in Fig. 6, which demonstrates a good match. These also match very well with the published results in [17].

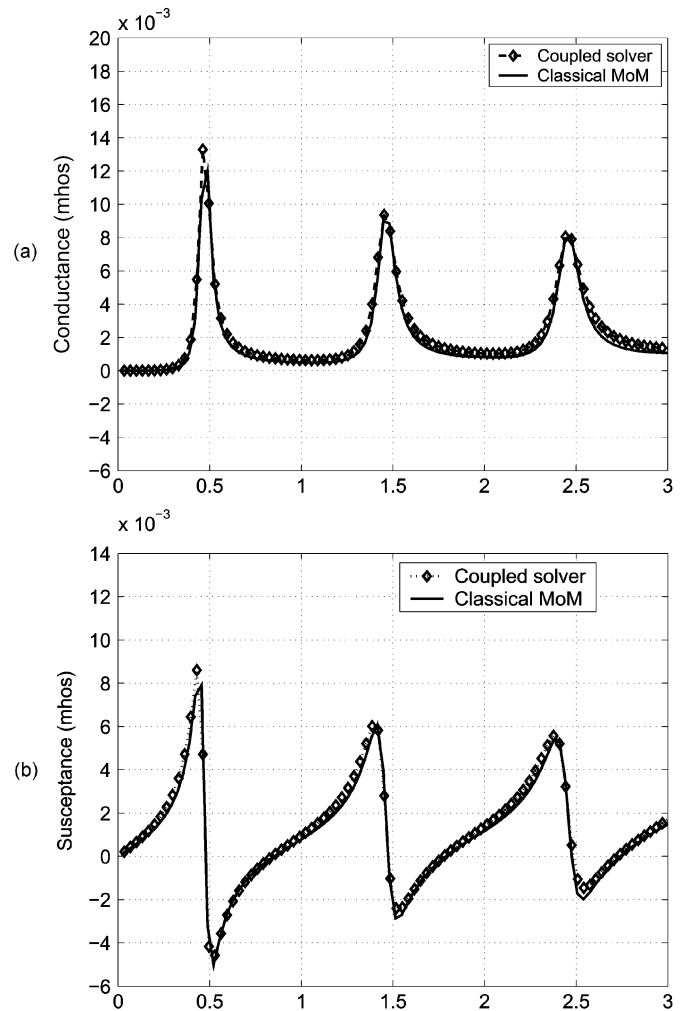


Fig. 6. Input conductance and susceptance versus l/λ . (a) Conductance. (b) Susceptance.

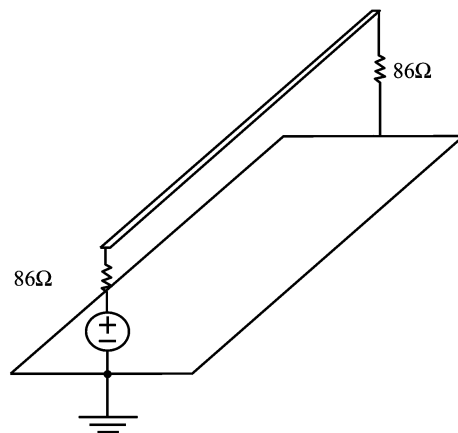


Fig. 7. Interconnect over a solid ground plane.

Another validation example, comparing the presented approach to the standard PEEC, is an interconnect over a ground plane, as in [29], and as shown in Fig. 7.

The ground plane is 2 cm long \times 1 cm wide and the trace is 2 cm long \times 1 mm wide and stays 0.5 mm above the ground plane. The frequency dependence of the input impedance is depicted in Fig. 8, and matches well. The small bump is very near

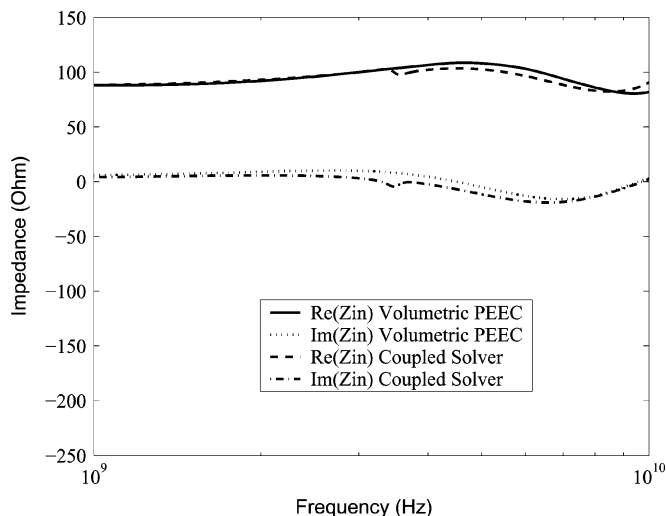


Fig. 8. Input impedance of an interconnect over a ground plane.

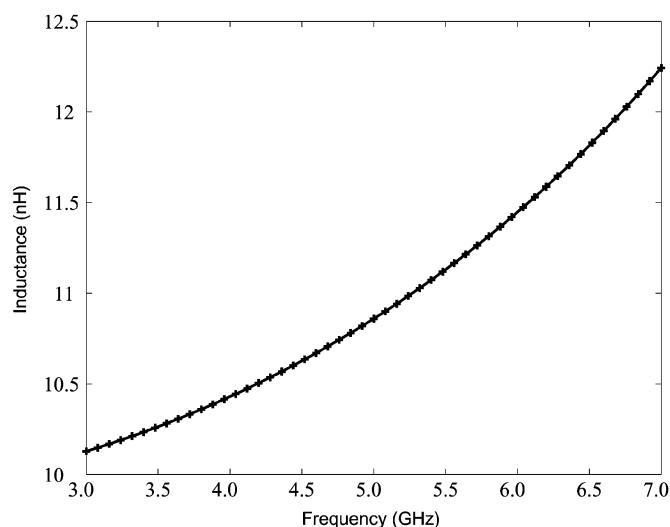


Fig. 10. Extracted equivalent inductance.

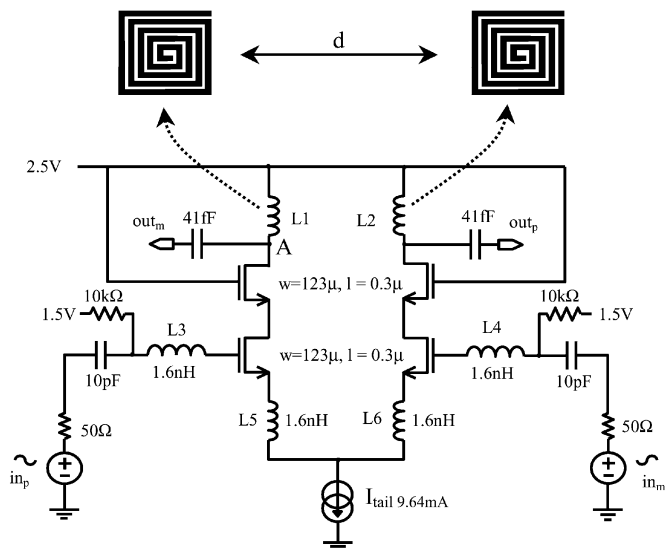


Fig. 9. Schematic of a 5.6-GHz LNA.

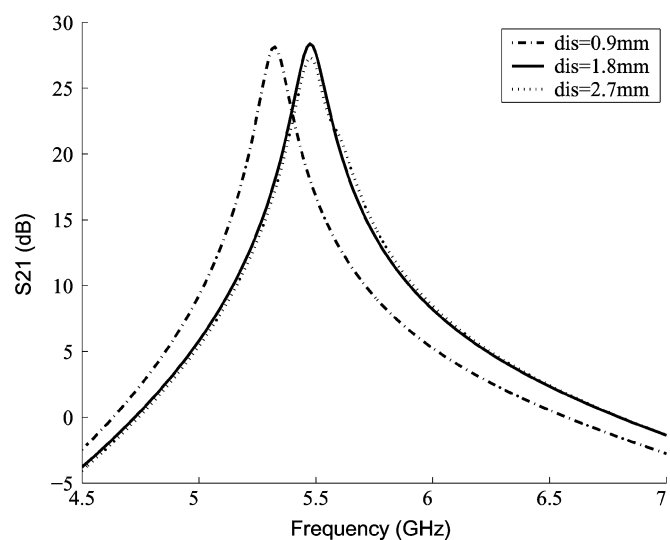


Fig. 11. S_{21} curve versus distance between inductors.

the first resonant frequency, and might be related to internal resonant effects in the EFIE system, but this is not clear.

One of the typical applications is circuit/layout co-simulation for RF electronics system design, where on-chip inductors are often employed. In RF circuit design, accurate characterization of the inductor is the most challenging task. Fig. 9 shows the topology of a 5.6-GHz differential-mode LNA, where several on-chip inductors are included either for the frequency-selection purpose such as $L1$ and $L2$ or for the impedance matching purpose such as $L3$ – $L6$.

With 5.6-GHz central working frequency, performance of the LNA will be affected by both the distributed effect and the crosstalk of on-chip spiral inductors. The precision of two inductors $L1$ and $L2$ is most important since it affects the central frequency where the maximum gain can be derived. While the transistor sizes are fixed by the requirement of the optimum noise figure [30] to be $123 \mu\text{m}$, the main design task is to adjust the turns and spacing of spiral inductors to tune the resonant frequency of the LC tank to the central frequency 5.6 GHz.

The spiral inductor $L1$ is first simulated using the coupled solver to decide the number of turns according to the extracted equivalent inductance. With a total parasitic capacitance to be 105 fF at node A, the inductor is designed to be five turns with an area of $500 \mu\text{m} \times 500 \mu\text{m}$. Fig. 10 shows the extracted equivalent inductance of such a single spiral inductor. The increase in inductance with frequency is due to approaching self-resonance frequency of the inductor.

Due to the radiation and inductive coupling effects, the two inductors will mutually couple, and lead to a shift in the central frequency. Fig. 11 shows a series of S_{21} curves versus different distances between the two inductors.

As the two inductors are moved closer, the coupling effect becomes prominent and leads to poorer performance. In actuality, the coupling effect could also be used to an advantage: due to the differential mode nature of the currents through the two inductors, a larger effective inductance can be realized by tight coupling between the two inductors. In other words, the same inductance value could be achieved using a lesser number

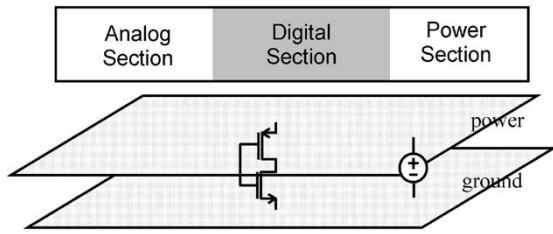


Fig. 12. Structure of a mixed-signal board with a noise source at the center.

of turns and, thus, less chip area. Some new multilevel inductor designs are based on this concept.

To simulate the coupled system in the frequency domain, an operating point analysis is first performed to linearize the nonlinear BSIM3 transistor model [31]. As an existing circuit simulation technique, the operating point is calculated via Newton–Raphson iterations. EM structures are not involved in those iterations directly; instead, these are represented by a resistance network calculated using a volumetric resistance extractor.

If large-signal analysis instead of the small-signal analysis presented above is required for the coupled system, the frequency domain can be facilitated through a harmonic-balance method [32] coupled to the EM simulation. However, this is beyond the scope of this paper.

A frequency sweep is then performed for the range of interest. The EM problem was meshed with 5120 RWG basis functions and it required 43 s to set up the problem and 88 s to solve using our in-house low-rank compression fast iterative solver on a 1.6-GHz Pentium processor. In contrast, extraction of the entire port model requires 42-s one-time setup time and 334-s solve time. Note that the solve time for port-model extraction is approximately four times as long as the solve time for the coupled solver, which is because the problem needs to be solved four times in order to extract the port model, each for one column of the Y matrix with a 1-V excitation on one port and 0-V excitation on the rest of ports.

The second example studies the power/ground-plane voltage bounce distribution due to a high-frequency noise source. Consider a typical mixed analog/digital print circuit board (PCB), as shown in Fig. 12.

Since digital circuits are usually associated with high-speed signal switching that contains numerous high-frequency components, the potential difference between power and ground planes will not be equal to ideal supply voltage everywhere. At high frequencies, the power and ground planes need to be considered as a distributed RLC network instead of ideal conduction planes. The voltage bounce could cause digital logic circuits to switch erroneously. In such a case, decoupling capacitors are needed to suppress the peak bounce voltage.

With traditional port-model-based EM–circuit simulation methods, it is difficult to acquire the voltage bounce distribution information all over the plane since the potentials can only be accessed via ports. Thus, deriving the spatial distribution of the potential requires ports everywhere on the plane and could make the problem cumbersome or too large to solve. On the other hand, since the coupled circuit–EM solver uses equivalent surface currents as system unknowns, the voltage/field

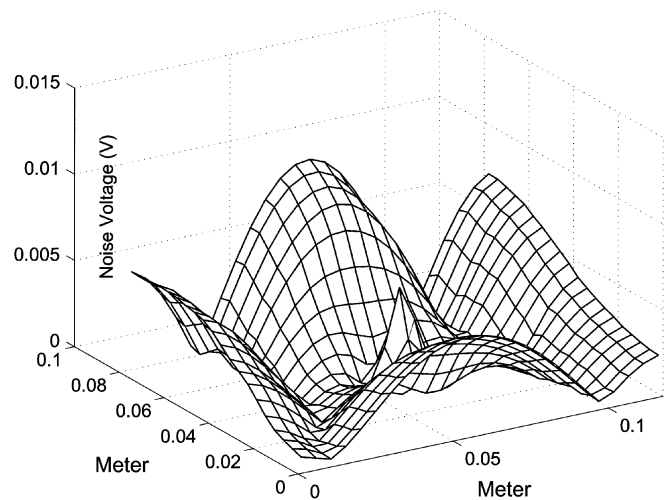


Fig. 13. Bounce-voltage distribution at 3 GHz.

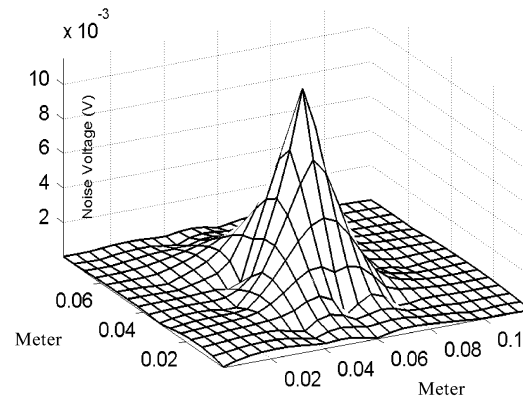


Fig. 14. Bounce-voltage distribution at 3 GHz after adding 20 decoupling capacitors.

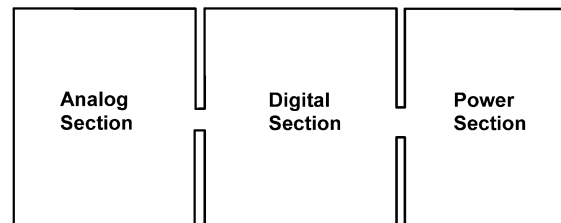


Fig. 15. Partially split power ground-plane design.

distribution can then be easily derived by a post-processing operation once the coupled system is solved.

In Fig. 12, the size of the PCB board is 12 cm \times 8 cm. At 3 GHz, 1-mA noise source at the board center can cause a bounce-voltage distribution, as shown in Fig. 13.

By continuously pinning down the peak bounce voltage using 10-nF decoupling capacitors, peaks of the noise voltage can be isolated in a local area of the noise source, as shown in Fig. 14, after adding approximately 20 decoupling capacitors.

Note that the EM part of the problem does not change as additional capacitors are added and, hence, the factorization and storage of the EM section can be done just once if required, using the *EM port model* of the coupled system.

An alternative design approach is to design the power/ground board, as shown in Fig. 15, with partially split planes.

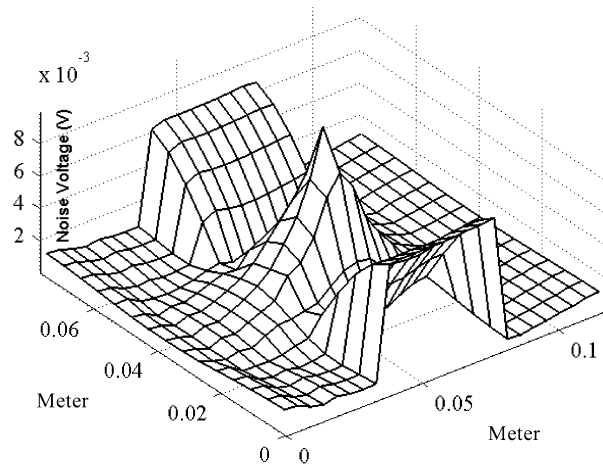


Fig. 16. Bounce-voltage distribution at 3 GHz for split power/ground plane.

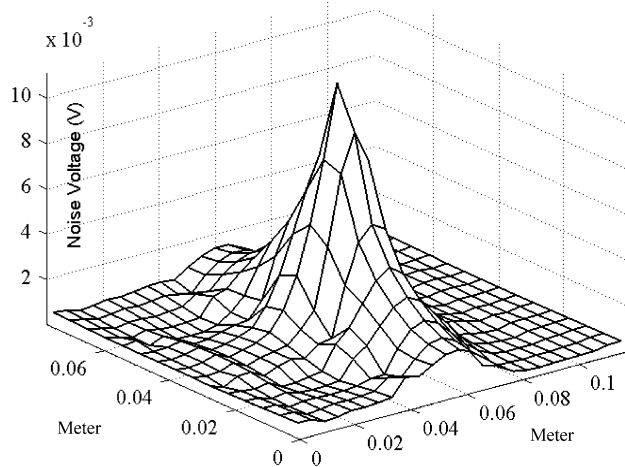


Fig. 17. Bounce-voltage distribution at 3 GHz for split power/ground plane with nine decoupling capacitor.

Simulation results reveal that the bounce-voltage localization effect was achieved even without adding decoupling capacitors, as shown in Fig. 16.

Further localization of bounce voltage will need a smaller number of decoupling capacitors compared to the previous example. Bounce localization shown in Fig. 17 was achieved by using nine decoupling capacitors.

VI. CONCLUSION

In this paper, a coupled circuit-EM formulation has been presented. The EM solution is based on full-wave surface integral equations (i.e., EFIEs), the circuit solution is based on KVL and KCL, and the coupling is ensured by charge and current continuity, as well as potential matching. The primary objective of the method is to ensure proper physics-based coupling between the circuit and the EM parts such that a coupled matrix can be formulated. While different kinds of EM and circuit port models can be derived, a fully coupled solution process will guarantee complete electrical transparency in the entire system, including all EM and circuit effects. Work in progress is aimed at extending the same approach to the time-domain simulation to in-

clude the effect of lossy conductors and to incorporate fast multilevel solvers and fast frequency-sweep methods for the coupled system.

REFERENCES

- [1] K. Kundert, H. Chang, D. Jefferies, G. Lamant, E. Malavasi, and F. Sendig, "Design of mixed-signal systems-on-a-chip," *IEEE Trans. Computer-Aided Design*, vol. 19, pp. 1561–1571, Dec. 2000.
- [2] I. Erdin and M. Nakhla, "Mixed circuit/electromagnetic analysis of field coupling to high speed interconnects in inhomogeneous medium," in *Int. IEEE Electromagnetic Compatibility Symp.*, vol. 1, Aug. 1999, pp. 446–449.
- [3] W. Sui, D. A. Christensen, and C. H. Durney, "Extending the two-dimensional FDTD method to hybrid electromagnetic systems with active and passive lumped elements," *IEEE Trans. Microwave Theory Tech.*, vol. 40, pp. 724–730, Apr. 1992.
- [4] R. Khazaka and M. Nakhla, "Analysis of high-speed interconnects in the presence of electromagnetic interference," *IEEE Trans. Microwave Theory Tech.*, vol. 46, pp. 940–947, July 1998.
- [5] M. N. Abdulla and M. B. Steer, "Extraction of network parameters in the electromagnetic analysis of planar structures using the method of moments," *IEEE Trans. Microwave Theory Tech.*, vol. 49, pp. 94–103, Jan. 2001.
- [6] A. Canova, M. Ottella, and D. Rodger, "A coupled field-circuit approach to 3D FEM analysis of electromechanical devices," in *IEEE 9th Int. Electrical Machines and Drive Conf.*, Sept. 1999, pp. 71–75.
- [7] M. Feliziani and F. Maradei, "Circuit-oriented FEM: Solution of circuit-field coupled problems by circuit equations," *IEEE Trans. Magn.*, vol. 38, pp. 965–968, Mar. 2002.
- [8] M. C. Costa, S. I. Nabeta, and J. R. Cardoso, "Modified nodal analysis applied to electric circuits coupled with FEM in the simulation of a universal motor," *IEEE Trans. Magn.*, vol. 36, pp. 1431–1434, July 2000.
- [9] P. P. M. So and W. J. R. Hofer, "A general framework for SPICE-TLM interconnection," in *IEEE MTT-S Int. Microwave Symposium Dig.*, vol. 2, June 2002, pp. 1123–1126.
- [10] S. Chun, M. Swaminathan, L. D. Smith, J. Srinivasan, Z. Jin, and M. K. Iyer, "Modeling of simultaneous switching noise in high speed systems," *IEEE Trans. Adv. Packag.*, vol. 24, pp. 132–142, May 2001.
- [11] A. E. Ruehli, "Equivalent circuit models for three-dimensional multiconductor systems," *IEEE Trans. Microwave Theory Tech.*, vol. MTT-22, pp. 216–221, Mar. 1974.
- [12] A. E. Ruehli, G. Antonini, J. Esch, J. Ekman, A. Mayo, and A. Orlandi, "Nonorthogonal PEEC formulation for time- and frequency-domain EM and circuit modeling," *IEEE Trans. Electromagn. Compat.*, vol. 45, pp. 167–176, May 2003.
- [13] A. Rong and A. C. Cangellaris, "Generalized PEEC models for three-dimensional interconnect structures and integrated passives of arbitrary shapes," in *Proc. Electrical Performance of Electronic Packaging Conf.*, vol. 10, Boston, MA, Oct. 2001, pp. 225–228.
- [14] Y. Wang, V. Jandhyala, and C. J. Shi, "Coupled electromagnetic-circuit simulation of arbitrarily-shaped conducting structures," in *Proc. Electrical Performance of Electronic Packaging Conf.*, vol. 10, Boston, MA, Oct. 2001, pp. 233–236.
- [15] M. Kamon, M. J. Tstok, and J. K. White, "FASTHENRY: A multipole-accelerated 3-D inductance extraction program," *IEEE Trans. Microwave Theory Tech.*, vol. 42, pp. 1750–1758, Sept. 1994.
- [16] G. Antonini, A. Orlandi, and A. E. Ruehli, "Harten's scheme for PEEC method," in *IEEE Int. Electromagnetic Compatibility Symp.*, vol. 1, Aug. 2001, pp. 340–344.
- [17] R. F. Harrington, *Field Computation by Moment Methods*. Malabar, FL: Krieger, 1982, pp. 71–72.
- [18] A. Odabasioglu, M. Celik, and L. T. Pileggi, "PRIMA: Passive reduced-order interconnect macromodeling algorithm," in *IEEE/ACM Int. Computer-Aided Design Conf. Tech. Dig.*, Nov. 1997, pp. 58–65.
- [19] K. Nabors and J. K. White, "FastCap: A multipole accelerated 3-D capacitance extraction program," *IEEE Trans. Computer-Aided Design*, vol. 10, pp. 1447–1459, Nov. 1991.
- [20] J. R. Phillips and J. K. White, "Efficient capacitance extraction of 3D structures using generalized pre-corrected FFT methods," in *3rd Electrical Performance of Electronic Packaging Topical Meeting*, Nov. 1994, pp. 253–256.
- [21] S. Kapur and D. E. Long, "IES³: A fast integral equation solver for efficient 3-dimensional extraction," in *IEEE/ACM Int. Computer-Aided Design Conf. Dig.*, Nov. 1997, pp. 448–455.

- [22] D. Gope and V. Jandhyala, "An iteration-free fast multilevel solver for dense method of moment systems," in *Proc. Electrical Performance Electronic Packaging Conf.*, vol. 10, Boston, MA, Oct. 2001, pp. 177–180.
- [23] Y. Wang, D. Gope, V. Jandhyala, and R. Shi, "Integral equation based coupled electromagnetic-circuit simulation in the frequency domain," in *Proc. IEEE AP-S URSI Symp.*, vol. 3, Columbus, OH, June 2003, pp. 328–331.
- [24] S. M. Rao, D. R. Wilton, and A. W. Glisson, "Electromagnetic scattering by surfaces of arbitrary shape," *IEEE Trans. Antennas Propagat.*, vol. AP-30, pp. 409–418, May 1982.
- [25] S. Chakraborty and V. Jandhyala, "Evaluation of Green's function integrals in conducting media," in *Proc. IEEE AP-S Symp. Dig.*, vol. 3, Columbus, OH, June 2003, pp. 320–323.
- [26] —, "Accurate computation of vector potentials in lossy media," *Microwave Opt. Technol. Lett.*, vol. 36, no. 5, pp. 359–363, Mar. 2003.
- [27] N. J. Champagne II, J. T. Williams, and D. R. Wilton, "The use of curved segments for numerically modeling thin wire antennas and scatterers," *IEEE Trans. Antennas Propagat.*, vol. 40, pp. 682–689, June 1992.
- [28] J. Vlach and K. Singhal, *Computer Methods for Circuit Analysis and Design*. New York: Van Nostrand, 1983.
- [29] W. Pinello, A. C. Cangellaris, and A. Ruehli, "Hybrid electromagnetic modeling of noise interactions in packaged electronics based on the partial-element equivalent-circuit formulation," *IEEE Trans. Microwave Theory Tech.*, vol. 45, pp. 1889–1896, Oct. 1997.
- [30] B. Razavi, *RF Microelectronics*. Englewood Cliffs, NJ: Prentice-Hall, 1997, ch. 6.
- [31] Y. Cheng and C. M. Hu, *MOSFET Modeling and BSIM3 User's Guide*. New York: Kluwer, 1999.
- [32] V. Rizzoli, A. Lipparini, A. Costanzo, F. Matri, C. Cecchetti, A. Neri, and D. Masotti, "State-of-the-art harmonic-balance simulation of forced nonlinear microwave circuits by the piecewise technique," *IEEE Trans. Microwave Theory Tech.*, vol. 40, pp. 12–28, Jan. 1992.



Yong Wang received the B.S. and M.S. degrees in electronics from Tsinghua University, Beijing, China, in 1994 and 1998 respectively, and is currently working toward the Ph.D. degree in electrical engineering at the University of Washington, Seattle.

From 1994 to 1996, he was a Research Assistant with the Circuit and System Laboratory, Tsinghua University, where he was involved with circuit simulation and macromodeling. From 1998 to 2000, he was with Analog Inc., where he was involved with modeling engineering. His research interests

include analog/mixed-signal circuit simulation, EM simulation, and analog design automation.



Dipanjan Gope (S'00) received the B.Tech. degree in electronics and electrical communication engineering from Indian Institute of Technology (IIT), Kharagpur, India, in 2000, the M.S. degree in electrical engineering from the University of Washington, Seattle, in 2003, and is currently working toward the Ph.D. degree in computational electromagnetics at the University of Washington.

He is currently a Graduate Research Assistant with the University of Washington. His research interests include combined circuit-EM simulations, signal integrity in high-speed circuits and devices, and fast solution algorithms.



Vikram Jandhyala (M'00–SM'03) received the B.Tech. degree in electrical engineering from the Indian Institute of Technology (IIT), Delhi, India, in 1993, and the M.S. and Ph.D. degrees from the University of Illinois at Urbana-Champaign, in 1995 and 1998, respectively.

As part of his graduate work, he co-developed the steepest descent fast-multipole method for rapid simulation of a large class of EM problems. From 1998 to 2000, he was a Research and Development Engineer with the Ansoft Corporation, Pittsburgh, PA. He was involved in the acceleration of Ansoft's integral-equation solvers, and co-developed a fast multipole-based extraction tool in Ansoft's SPICELink versions released in 1999 and 2000. Since 2000, he has been an Assistant Professor with the Electrical Engineering Department, University of Washington, Seattle. He directs the Applied Computational Electromagnetics Laboratory, with research interests and projects in several areas of computational electromagnetics, including fast solvers and integral-equation formulations in the frequency and time domains, high-speed circuits and devices, coupled multiphysics simulation, novel materials, and propagation. He has visiting research status with the Lawrence Livermore National Laboratories. He has authored or coauthored over 70 journal and conference papers.

Dr. Jandhyala is a full elected member of the International Scientific Radio Union (URSI) Commission B. He has served as a reviewer for several IEEE journals and conferences and national and international proposal panels. He is on the Technical Program Committee of the IEEE Design Automation Conference and the IEEE Antennas and Propagation Society (IEEE AP-S) Symposium. He was a recipient of the 2001 National Science Foundation (NSF) CAREER grant, a 1998 Outstanding Graduate Research Award presented by the University of Illinois, and a 1996–1997 IEEE Microwave Graduate Fellowship.



C.-J. Richard Shi (M'91–SM'99) is currently an Associate Professor of electrical engineering with the University of Washington, Seattle. He is a key contributor to IEEE Standard 1076.1-1999 (VHDL-AMS) for the description and simulation of mixed-signal circuits and systems. His research interests include several aspects of the computer-aided design and test of integrated circuits and systems, with particular emphasis on analog/mixed-signal and deep-submicrometer circuit modeling, simulation, and design automation.

Dr. Shi founded the IEEE International Workshop on Behavioral Modeling and Simulation (BMAS) in 1997. He has served on the Technical Program Committees of several international conferences. He has been an associate editor, as well as a guest editor, for the IEEE TRANSACTIONS ON CIRCUITS AND SYSTEMS—II, ANALOG AND DIGITAL SIGNAL PROCESSING. He is currently an associate editor of the IEEE TRANSACTIONS ON COMPUTER-AIDED DESIGN OF INTEGRATED CIRCUITS AND SYSTEMS. He was the recipient of a Best Paper Award presented by the IEEE/Association for Computing Machinery (ACM) Design Automation Conference, a Best Paper Award presented by the IEEE Very Large Scale Integration (VLSI) Test Symposium, a National Science Foundation CAREER Award, and a Doctoral Prize presented by the Natural Science and Engineering Research Council of Canada.